HARDWARE-IN-THE-LOOP SIMULATION OF FUEL-CELL-BASED HYBRID-ELECTRICAL UAV PROPULSION

Dries Verstraete*, James R. Harvey, Jennifer L. Palmer****

*** School of Aerospace, Mechanical and Mechatronic Engineering**
The University of Sydney, Aeronautical Eng Bldg J11, NSW 2006 Australia
****Air Vehicles Division, Defence Science and Technology Organisation,**
506 Lorimer St., Fishermans Bend VIC 3207 Australia
Dries.Verstraete@sydney.edu.au; James.Harvey@dsto.defence.gov.au;
Jennifer.Palmer@dsto.defence.gov.au
Keywords: *hardware-in-the-loop simulation, fuel cell, hybrid-electrical propulsion, unmanned air vehicles, unmanned aircraft systems*

Abstract

This paper presents the experimental architecture and test results of a hardware-in-the-loop (HWIL) simulation of a fuel-cell-based hybrid-electrical propulsion system for small-scale unmanned aerial vehicles (UAVs). The Aeropak system from Horizon Energy Systems was tested dynamically and electrical loads were applied to emulate the conditions of operation in flight. Experimental results from HWIL testing of the fuel-cell-based power train are presented and discussed. The results clarify the functioning of the power-management board of the Aeropak system and the influence of purging and short-circuiting on its operation. The results also show that fuel-cell dynamics can have a significant impact on mission performance. Dynamic tests showed that the fuel cell can temporarily produce a higher over-potential than observed during static tests. This confirms the importance of HWIL simulations for accurate performance predictions of fuel-cell-powered UAVs.

1 Introduction

Small-scale, electrically powered unmanned aerial vehicles (UAVs) are currently in use for a variety of reconnaissance and remote-sensing missions. For these aircraft, electrical propulsion is generally preferred over small reciprocating engines or gas turbines because of the latter's low efficiencies at small sizes [1].

Electrical propulsion furthermore offers low vibration levels, quiet operation, and physical robustness. The mission duration is limited, however, by the energy density of existing batteries. Current lithium-polymer (Li-Po) batteries possess an energy density of 150–200 W-hr/kg [2, 3], which provides a typical small UAV with an endurance of 60–90 mins. In contrast, a compressed-hydrogen tank with a 6% hydrogen-storage weight fraction, capable of providing fuel for a fuel cell or internal combustion engine, has an energy density in excess of 800–1000 W-hr/kg [2, 3].

A desire for longer endurance than is available from the current generation of batteries has motivated the development of fuel-cell-based electrical-propulsion systems. These advanced power-plant designs, however, present implementation challenges that require new development methods and tools. Fuel cells, for instance, generally have low specific power (W/kg), compared with internal combustion engines; whereas high specific power is required to improve aircraft (speed) performance and manoeuvrability. Aircraft concepts powered solely by fuel cells therefore require both extremely lightweight airframes and low-power payloads and still result in designs that are highly constrained operationally [4].

A hybrid-electrical propulsion chain with secondary power sources having high specific power (*e.g.*, batteries or ultracapacitors) to provide a brief high-power capability could allevi-

ate those restrictions and lead to a platform with a better overall performance [5-7]. Several successful demonstrations have shown the feasibility of fuel-cell-powered UAVs, and several fuel-cell-powered UAVs are now commercially available [8, 9]. Despite this, little data is available regarding the detailed performance of these aircraft and their power plants [10, 11].

To develop a comprehensive understanding of the challenges associated with the use of fuel-cell-based, hybrid-electrical propulsion systems for UAVs, a dedicated test bench for hardware-in-the-loop (HWIL) simulations has been developed. This paper describes the HWIL test bench, which was built around an Aeropak hybrid system with a 200-W polymer electrolyte membrane (PEM) fuel cell from Horizon Energy Systems [12], and gives results for simulations based on flight data of a small unmanned aircraft [13].

Section 2 of this paper gives an overview of the data available in the public domain on small fuel-cell-powered UAVs and their propulsion systems. Section 3 details the HWIL simulation architecture, both in terms of hardware and software. In Section 4, results of various runs of the HWIL simulator are given. These include initial tests to verify the manufacturer's polarisation-curve and fuel-consumption data, as well as flight simulations.

2 Research and Development of Fuel-Cell-Powered Aircraft

PEM fuel cells relying on hydrogen as fuel have been most commonly used in UAVs [14], with few exceptions [15]. Their advantages over other fuel-cell chemistries, with respect to mobile applications, include low operating temperatures that permit a short start-up time and relative compactness due to the thinness of their membrane electrode assemblies. Furthermore, the cells can operate with any orientation and do not utilise corrosive fluids [16]. Solid-oxide fuel cells share some of these advantages [17] and have also proven resistant to damage [18] from the mishaps typical of small UAVs.

Numerous reports from universities, governmental research organisations, and commercial entities illustrate the widespread interest in and strong prospects for the use of fuel cells on aircraft. Efforts to develop high-altitude, long-endurance (HALE) UAVs with hybrid-power systems relying on solar and fuel cells, to act as pseudo-satellites for months- or years-long surveillance, have been on-going for more than a decade in the US [19-21] and Europe [22-26]; and several studies have aimed to enable fuel-cell-powered aircraft for commercial transport [7, 27-33] and general aviation [34, 35].

Small, tactical UAVs, having wingspans of ~1–4 m and designed for portability and operation during surveillance missions by one or two people [14], have been a focus of recent research because of the several-fold increase in endurance fuel cells can provide [3, 14, 36]. These efforts have been enabled by, and have helped broaden, the availability of miniaturised fuel-cell systems [8, 9, 37-40]. Recent demonstrations have been performed with commercially available UAVs, including Malat's Bird Eye 650 [8], Elbit Systems' Skylark [8], Uconsystem's Remo Eye-006 [8, 41], BlueBird's Boomerang [8, 42], Aerovironment's Puma [38, 43], Robota's Robosoar [9], and L-3's Mako [44]; and the potential for fuel cells to improve their range and endurance over that available with Li-Po or Li-primary batteries has been documented [3, 36]. Fuel-cell-powered UAVs are available in the marketplace for military and commercial applications, though the cost of components has limited their adoption.

Flight demonstrations of fuel-cell-powered surveillance-type UAVs have also been reported by university and governmental researchers. The US Naval Research Laboratory developed and tested the Spider Lion [45-47] and Ion Tiger [38, 48] aircraft; and academic projects have resulted in the construction and trial of Hy-Fly at the University of Applied Sciences in Wiesbaden, Germany [49], Pterosoar at California State University in Los Angeles [8, 50, 51], and Endurance, powered by a solid-oxide fuel cell, at the University of Michigan [52, 53]. Fuel-cell UAVs have also been developed and demonstrated by researchers at the Korea Advanced Institute of Science and Technology (KAIST) and Chosun University [54], at the Georgia Tech Research Institute [10, 11, 55, 56], and at Colorado State University [57].

Other notable developments include flight demonstrations of more unusual designs, such as Aerovironment's 0.38-m-wingspan Hornet flying wing [58-60] and the 1-m HyFish jet by the German Aerospace Center (DLR) [8, 61].

Most of the trial reports and published design studies of various classes of UAVs [5, 25, 62-66] provide only "high-level" conceptual aircraft designs. The necessary "low-level" compromises between aircraft requirements and the characteristics of the power plant are not addressed, though some efforts have been made to develop design methodologies that encompass these considerations [67-69]. Detailed descriptions of the design and performance of the structure and subsystems used in fuel-cell-powered aircraft are scarce [10, 24, 26, 50, 57, 70, 71], as are comparisons of aircraft-design parameters and flight-trial results [54, 72] and HWIL simulations [73].

Aside from the documented aircraft development and testing, research to enable better and more widespread use of fuel cells on aircraft is being carried out globally. For example, lightweight, high-powered motors made of high-temperature superconducting materials are being developed with the goal of providing propulsion systems with higher power density for high-altitude use [27, 74]; and greater understanding of the effects of high altitude on fuel-cell performance is being pursued [75].

Although the expense of fuel cells, issues surrounding high-density hydrogen storage, and the need for hydrogen infrastructure currently limit their broad application, research is being undertaken to develop and prove efficient hydrogen-storage materials for aerospace applications [54, 71, 76-79]. In addition, dynamic-power-management strategies are being applied to hybrid power systems to increase their overall performance and improve their reliability and usefulness [80].

3 Hardware-in-the-Loop Architecture

In HWIL simulation, the physical hardware of a subsystem of a dynamic system is immersed within a closed-loop virtual simulation of the remaining subsystems. Interface components between the hardware and software allow for a bidirectional flow of information among the physical and virtual systems [73, 81]. HWIL simulation can be a very effective tool for performance characterisation of complex power plants for unmanned aircraft as data-acquisition (DAQ) hardware that is not flight worthy can be used and test conditions can be more rigorously controlled [73]. As a consequence, the experimental uncertainty can be much lower than for flight-testing.

The selection of a HWIL architecture consists firstly of determining which components will be represented in hardware and which in software. This obviously depends on the purpose and scope of the simulation. For the current HWIL test bench, the fuel-cell stack and controller, Li-Po batteries and power-management board of the Aeropak system were selected as physical components on the bench, as shown in Fig. 1. In a next step, the HWIL bench will be expanded to include the motor and speed controller.

As shown in Fig. 1, this hardware was supplemented with a DAQ system that formed the interface with the software component of the architecture. Below, the simulation hardware, the DAQ components, and the simulation software are briefly described.

3.1 Simulation Hardware

During the current HWIL test sequence, the hardware components were mounted on the laboratory bench top and connected electrically.

The Aeropak hybrid system, shown in Fig. 2, was the only source of electrical power for the aircraft components during testing. The

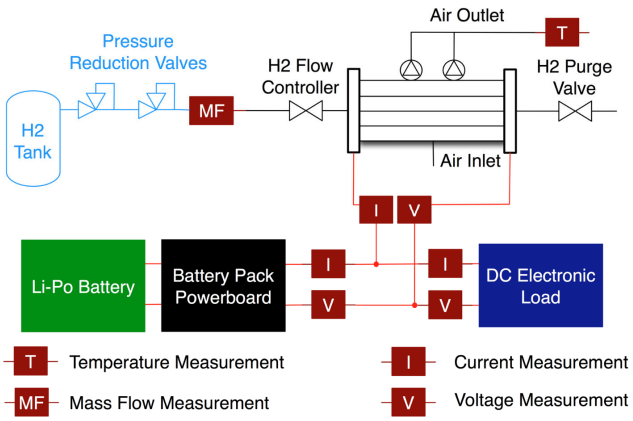

Fig. 1. Test-bench schematic.

system consists of a 35-cell PEM fuel cell and a 6-cell 1350 mA-hr Li-Po battery pack. The fuel cell can deliver up to 10 A of current and has a nominal power output of 200 W. Its operating voltage ranges from 32 V (no load) to 21 V (full load). The fuel cell is self-humidified and air-cooled and only requires near-ambient cathode pressure. The hydrogen side (anode) is dead-ended, meaning all the hydrogen entering the anode compartment is either consumed by the fuel-cell reaction or wasted due to leakage.

As shown in Fig. 1, the fuel-cell controller adjusts the temperature of the stack by dictating the speed of the cathode supply fans. Increasing the cathode flow rate increases the evaporative cooling of the stack and reduces its temperature. The controller also regulates periodic anode purging to maintain a high rate of hydrogen utilisation and to ensure prolonged stack performance [12]. Anode purging is required to remove inert gases, liquid water and contaminants, as well as any excess hydrogen from the fuel-cell anode, and to maintain internal pressure at appropriate levels [73, 81]. Finally, the con-troller short circuits the fuel cell every 10 s. This short circuiting is built into the fuel-cell controller to increase the stack efficiency and forms part of its self-humidification process [8]. Short circuiting is executed through a solid-state switch on the controller that is connected across the fuel-cell stack and the load. During short circuiting, the load is disconnected for about 50 ms, and the fuel cell does not supply power to either the load or its own controller [8]. The hybrid battery is included in the circuit to provide continuous power to the load and controller and to prevent total loss of power to either. The fuel-cell controller has a capacitor to supplement the power output, but its capacity is not sufficient to bridge the 50-ms gap completely [8].

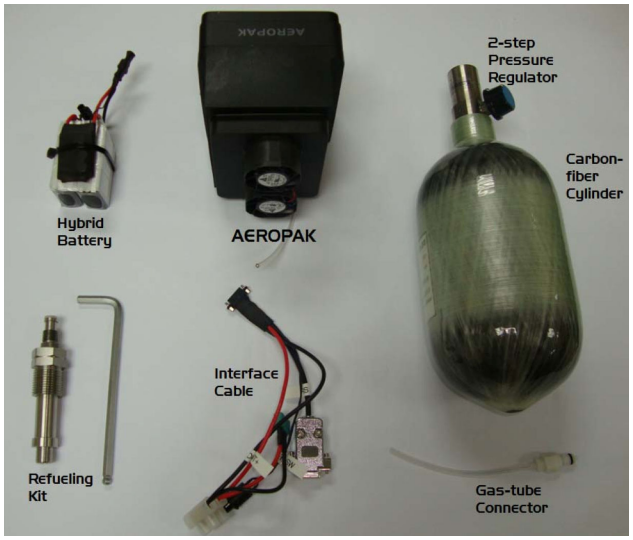

Fig. 2. Components of the hybrid Aeropak fuel-cell/Li-Po battery system from Horizon Energy Systems.

Besides bridging the short-circuiting period, the battery pack can deliver an additional 400 W for 2 min to meet the high-power requirements during UAV take-off or climbing [12]. The power-management board combines the total power output from the fuel cell and battery before delivering it to the load and is limited to 800 W for ~1 min to prevent its diode from overheating [12]. The board additionally recharges the battery when excess power is available from the fuel cell. The Aeropak system also comes with an interface cable that allows the user to input several system parameters through a serial connection. Table 1 lists each parameter, its range, and resolution. The parameters are communicated to the Aeropak's control board at ~1 Hz.

Table 1. Aeropak interface parameters [12]

Parameter	Range	Resolution
Stack voltage [V]	18–35	0.1
Stack current [A]	0–12	0.1
Fuel-cell power [W]	0–650	1
Total energy [W-hr]	0–1000	1
Stack temperature [°C]	0–70	0.1
Battery voltage [V]	18–30	0.1
Hydrogen pressure [bar]	0–10	0.1

3.2 Interface and Data-Acquisition Components

In the experimental arrangement described here, the interface components provided the physical and communication link between the simulation software and the previously described hardware components. The electrical connection between the hybrid Aeropak system and the simulation software was made by use of an ITECH Electronics IT8514F-1200 DC electronic load [82]. This programmable multi-mode load can draw up to 1200 W and is rated up to 120 V and 240 A. In constant-power mode, the load has an accuracy of 1.0% ± 0.1% of the full scale (FS)

[82]. For the current tests, the load was controlled at 5–10 Hz.

The power to be drawn from the fuel cell was determined from the aircraft-simulation package, taking the efficiency of the motor and propeller into account. As the Aeropak system does not provide a measurement of the hydrogen flow rate, a mass-flow meter was added to the test bench, so that the efficiency of the fuel-cell system could be determined. An Apex AX-M4SLPM-D5 flow meter was selected because it offers a high repeatability (±0.2% FS), coupled with a very high accuracy (±0.2% of the reading), when custom calibrated. As shown in Fig. 1, additional current and voltage measurements will be made to verify the parameters of the Aeropak and to reduce measurement uncertainty. When testing at low power, an ISO-TECH IDM73 multimeter will be used and its data was logged using a serial connection. The multimeter has a precision of ±1.0% for DC-current measurements and ±0.5% for voltage measurements. At higher currents, Eagle Tree Hall sensors will be used. They measure 0–100 A in 50 mA increments and can be calibrated before each test.

3.3 Simulation and Data-Acquisition Software

The DAQ software formed the interface between the hardware and the simulator software. It was written in Matlab, and the Matlab/Simulink environment was used to send all required commands to the electronic load and to acquire the data through serial ports. The Aeropak sends its data at a frequency of ~1 Hz, which is pre-programmed in the controller. The data from the mass-flow meter (temperature, pressure and mass-flow rate) was sampled at 20 Hz, whereas the output of the electronic load was sampled at 10 Hz. This permitted the capture of some of the transients that occurred when the fuel cell purged or short circuited.. During future tests with the Eagle Tree sensors, the frequency of the sampling will be increased to allow more accurate capturing of the transients. The communication with the electronic load was, however, too slow to allow that in the current set-up. The frequencies were thus halved for the long-endurance flight simulations. This was deemed adequate for modelling the aircraft dynamics and fuel consumption [73].

The simulator software translated the effect of the propeller, airframe, and flight controller to the power-train hardware. During initial testing performed for validation of the communications and benchmarking of the fuel-cell performance, power profiles were pre-programmed in the communication interface. In future tests, the hardware will be connected to a six-degree-of-freedom flight-simulation environment [83] that can compute the required thrust and propeller speed for given (commanded) aircraft altitude, airspeed and climb angle. The power required from the system can then be determined by use of propeller and motor models.

4 Test Results

4.1 Polarisation Curve

As explained previously, the fuel cell's control system regulates the temperature and evaporative cooling of the stack through the speed of the cathode-supply fans. This connection between the air-supply, water-management, and cooling systems leads to a nonlinear relationship between cathode stoichiometry, membrane humidification, and stack temperature [73]. This nonlinear relationship is to some extent represented by the so-called polarisation curve, which describes the "static" performance of the fuel-cell stack. The polarisation curve was determined by measuring the stack current and voltage at various power settings between 0 and 300 W for ~100 s, with the fuel cell operated under its normal thermal and stoichiometric control. The power was limited to 300 W to avoid draining the battery during the 100-s period. A high depletion rate would lead to fluctuations in the battery voltage during the testing period that would change its operating point. As a consequence, the maximum current during the "static" tests was restricted to ~11 A

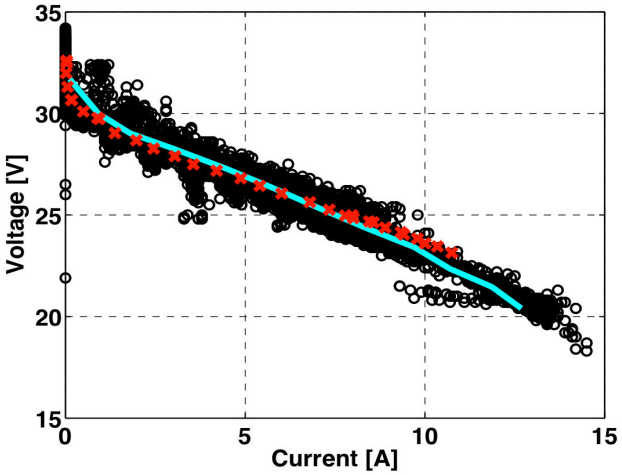

Fig. 3. Polarisation curve.

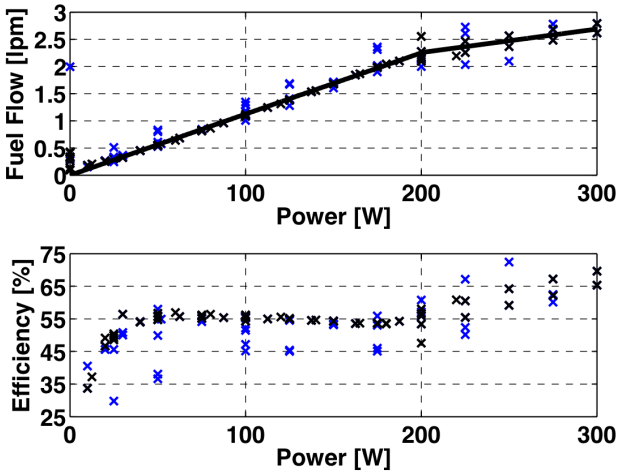

Fig. 4. Fuel consumption and fuel-cell efficiency.

The resulting polarisation curve is represented in Fig. 3. The time-averaged voltage and current over the 100-s period are shown as red crosses, and the black circles represent individual current–voltage combinations measured during fourteen tests. The cyan line, on the other hand, denotes the polarisation curve as given by the manufacturer [12]. As shown, the measured polarisation curve matches the curve from Ref. [12] closely, except at higher power (current) levels. The figure also clearly shows that a large variation exists between individual measurements. This was partially attributable to the fact that some points were measured as transients, where the fuel cell did not have time to stabilise its operation. The spread was, however, also related to the purging and short-circuiting of the fuel cell as shown in Section 4.3.

4.2 Fuel Consumption

The nominal fuel consumption of the fuel cell is given as 2.2 ℓ/min at standard conditions (sℓ/min) by the manufacturer [12]. According to Ref. [12], the fuel consumption varies linearly with power during steady-state operation. As the fuel consumption has been specified at only four power levels, additional power settings were used to obtain the fuel consumption as a function of power; and the results are shown in Fig. 4. The black symbols indicate "stationary" points, where the power level was maintained for a sufficiently long period to ensure that transient effects were negligible. The blue symbols indicate "transient" points, where the power was maintained for a relatively short period.

As Fig. 4 shows, the stationary fuel consumption was nearly linear up to 200 W, with a fuel consumption of approximately 2.25 sℓ/min at 200 W. Above 200 W, the slope of the fuel-consumption curve changed as the battery began to contribute to the delivered power. At 300 W, the consumption was ~2.69 sℓ/min. At higher power settings, the fuel consumption levelled off at ~3 sℓ/min. At that setting, the fuel cell supplied around 270 W; and the remainder of the demanded power came from the battery. During transients, the fuel consumption varied significantly from the steady-state value.

Figure 4 also gives the efficiency of the fuel cell for the measured operating points. The efficiency of the fuel cell, η_{FC}, is defined as the fraction of the lower heating value (*LHV*) of hydrogen that is transformed into useful power:

$$\eta_{FC} = \frac{P}{\dot{m}_f \cdot LHV}, \qquad (1)$$

where P is the power delivered by the system, and $\dot{m}_f$ is the fuel-flow rate. As shown, the efficiency hovered around 55% at ~40–200 W. Below this range, the efficiency dropped rapidly as the purging of the system became more dominant. Above 200 W, the efficiency rose, as it was based on the total power delivered by the hybrid system. As the battery delivered a share of the total power, this definition was no longer valid (and led to a computed efficiency of 125% at 600 W). During transients, the efficiency was typically 10% lower than the stationary value.

4.3 Results of Test Runs

The first test runs were aimed at gaining an understanding of the influence of the fuel-cell controller on the behaviour of the hybrid Aeropak system and its dynamic performance. The first test was used to explore the operation of the fuel cell at various power ratings. For the second test, the start-up sequence and the purging and short-circuiting of the system were examined in detail.

Figure 5 shows the power history of the first test. The black line indicates the programmed profile sent to the electronic load. The blue line gives the fuel-cell power, and the red line shows the power delivered by the battery. The green line is the sum of the power from the fuel-cell and battery. As shown, after about 100 s, the demanded power increased in steps of 100 W, up to 500 W. Each power setting was held for 30 s. Above 500 W, the power drawn by the load was increased by 50 W and then by 25 W for two more steps and only held for a short time. This was done to ensure that the battery would not be fully depleted during the test. During the final 300 s of the test, three peak-power bursts and a few smaller fluctuations were commanded to assess the reactivity of the system and to gain insight in the charging of the Li-Po battery.

Figure 5 shows that the fuel cell followed the requested power profile closely for the most part, though significant transient fluctuations occurred. It has to be noted that the apparent difference between the total and requested power levels at 370–600 s is artificial. In reality, the total power delivered from the system matched the requested power (with the exception of the peak fluctuations). During that time, the power drawn from the system was lower than the nominal power of the fuel cell, which resulted in recharging of the battery. To clearly indicate the periods when the battery was recharging, the sign of the current (and power) measured in the battery leads is not inverted. As a consequence, the power delivered to the battery is added to that delivered by the fuel cell, instead of being subtracted. This effect is also present during the low-power periods after 600 s.

Figure 6 shows the evolution of the current and voltage of the fuel cell and battery for the same test. It can be seen that the battery voltage (in red) dropped quickly when current was drawn from it. Due to the presence of the diode on the power-management board, the fuel-cell voltage (in blue) followed the battery voltage with a difference of ~1.0–1.5 V. At the peak power of 600 W, the battery voltage dropped below 20 V; and the battery delivered a current of ~15 A. When the current draw decreased, the battery voltage rose quickly. This does not indicate that the fuel cell was charging the battery, but was a consequence of a lower current being drawn from the battery. It was only at ~380 s, when the voltages differed by more than 1 V, that the system began to recharge the battery.

Figure 6 also shows that significant spikes in battery current occurred. These spikes occurred when the fuel cell was short circuited. At

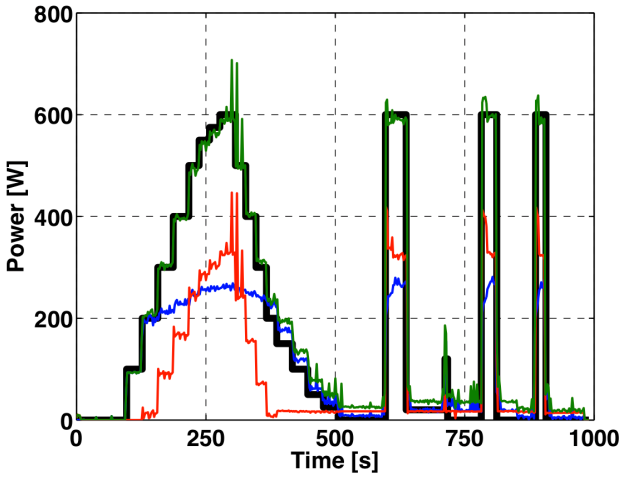

Fig. 5. Power as a function of time.

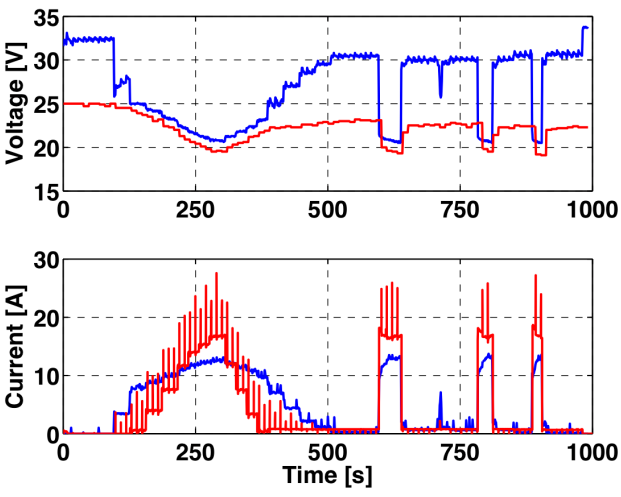

Fig. 6. Current and voltage history.

that point, the battery delivered the power that would normally come from the fuel cell, which resulted in a short, sharp increase in current delivered from the battery. The transient tests starting at ~600 s, in contrast, showed that the use of the battery was vital to the responsiveness of the system. As shown, the fuel cell was slower to transition to the higher power and the battery compensated by initially delivering a slightly higher current.

The start-up transient of the fuel cell was also examined. Figures 7 and 8 give results for the first 200 s of a test. The blue and red lines in Fig. 7 represent the values reported by the fuel cell, whereas the black lines denote the values registered by the electronic load. As shown in Fig. 7, the fuel cell was started up at ~12 s. During the start-up, the fuel-cell controller disconnected the fuel cell from the load; and at 20 s, when the fuel cell had stabilised at its zero-power operating point, the electronic load registered the fuel-cell voltage.

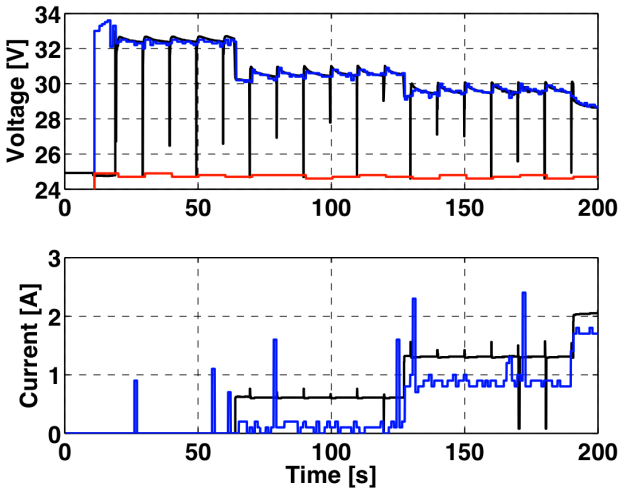

Fig. 7. Start-up evolution of current and voltage.

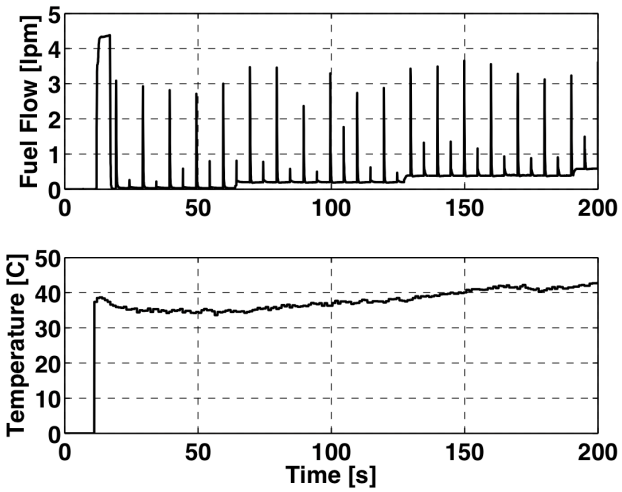

Fig. 8. Fuel flow and temperature during start-up.

Figure 7 clearly shows that the fuel-cell voltage followed a "sawtooth" pattern that was repeated every 10 s. The voltage decreased slightly over each 10-s period, until the fuel cell was short-circuited. At that point, the voltage was restored to its original value. Fig. 7 also indicates that the current reported by the fuel cell was considerably lower than the value registered by the load. This difference disappeared at ~60 W and was noted consistently throughout the testing. Further testing with the Eagle Tree sensors will be used to determine whether this phenomenon was related to the precision of the fuel cell's current sensor or whether the battery supplied current under these conditions.

When the fuel cell started-up, the fuel-flow rate increased significantly for ~8 s, as shown in Fig. 8. During that period, ~4.3 sℓ/min was consumed by the fuel cell. Afterward, the flow rate dropped to its stationary value. This increased mass flow brought the temperature of the fuel cell rapidly to its operating level, preventing damage to the membranes. Once started, the temperature dropped to its nominal value, after a small overshoot. Subsequent tests of longer duration at a given power rating showed that the controller regulated the fuel-cell temperature as a function of the power delivered. The temperature varied between 35 °C and 55–60 °C.

Besides the initial peak in fuel flow, several other sharp increases in the fuel-flow rate can be seen in Fig. 8. These peaks were related to the purging and the short circuiting of the fuel cell. During purging, there was a sudden change in pressure in the fuel lines. Whereas the mass-flow meter measured pressure to convert the volume-flow rate to a mass-flow rate, it is unclear whether the dynamic effect of this sudden pressure change or the inertia of the mass-flow meter influenced the readings. The peaks were fairly high, but only occurred for about 50 ms, so they represented only a small fraction of the total mass flow.

4.4 Flight-Simulation Results

Once the DAQ interface was developed, several long-duration missions, typical for small UAVs, were simulated. The missions consisted of a warm-up period at zero power, a maximum-power (600-W) climb, followed by a 200-W climb to the cruising altitude. Once at the cruising altitude, the UAV either loitered at a relatively low power (100 W) or performed a fast cruise (at 180 W). During descent, the motor was returned to zero power. During the final approach, flare, and runway taxying, 100 W was assumed to be used for 30 s before the fuel-cell power was set to 0 W and the fuel cell was turned off. These power profiles were adopted from simulations performed by use of DSTO's six-degree-of-freedom flight-simulator and based on flight data from the Kahu UAV [13]. The required power profiles were adjusted to account for the increase in fuselage volume required to store the fuel-cell and a hydrogen-storage tank. Whereas the Aeropak system is capable of longer sustained flights, the duration of the cruising and loitering phases were limited to 1 hr, as the transition effects between flight phases disappeared within that timeframe.

Figures 9, 10, and 11 give results for the mission with a 1-hr loitering phase. Fig. 9 shows the evolution of current and voltage during the mission. The red line indicates the battery voltage, whereas the multi-coloured line represents the voltage supplied by the fuel cell. Each flight phase is given in a different colour to allow a better distinction of the phases on the polarisation curve of Fig. 10. Figure 9 shows that it took ~14 min in the loitering phase for the fuel cell to settle to the steady-state power rating. During that period, the fuel cell was recharging the batteries that were significantly depleted during the 90-s, 600-W initial climb. After 20 min, the battery voltage remains steady at 23.4 V up to the descent phase. At the start of loiter, the voltage was at 22.6 V. At the start of descent, when the power is reduced to zero, the battery is recharged again as more spare power is available. At the end of descent the battery voltage has risen to 24.1 V.

Figure 10 shows the evolution of voltage and current on the polarisation curve. The figure clearly indicates that the performance of the fuel cell during transients differed significantly from its steady-state performance, which confirms the observations made from Fig. 3. After the initial start-up, the power was suddenly ramped up to 600 W, which caused the voltage to drop below the steady-state curve at point 1. As shown in Fig. 11, this corresponded to a point where the temperature exceeded the "equilibrium" tem-

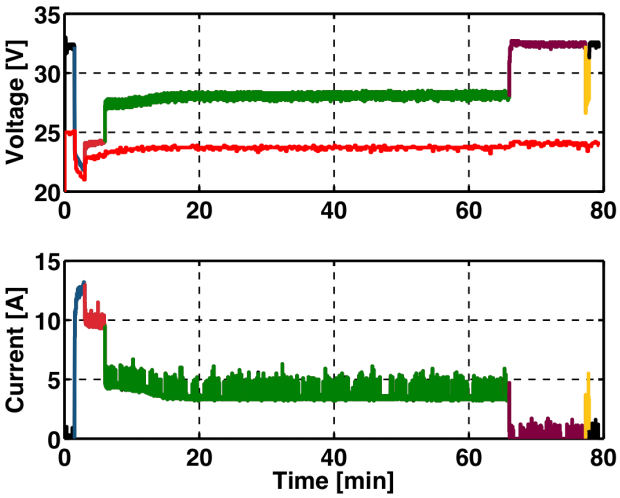

Fig. 9. Evolution of current and voltage during the endurance mission.

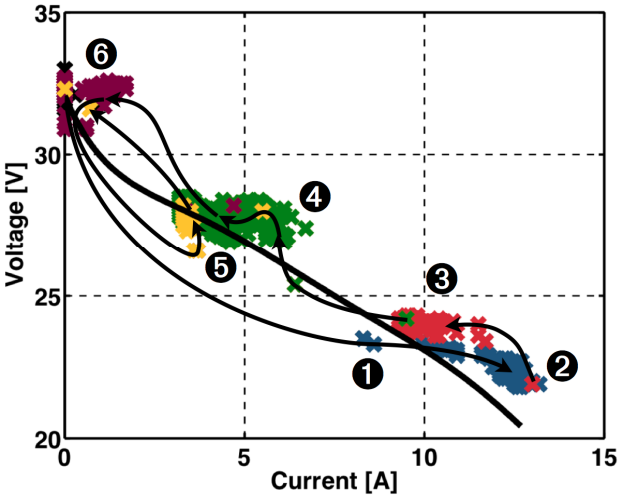

Fig. 10. Polarisation curve for the endurance mission.

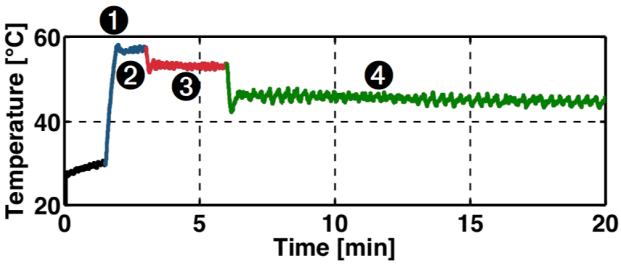

Fig. 11. Temperature evolution at the beginning of the endurance mission.

perature for that particular power rating. The fuel-cell controller sped up the fans and the current increased until the fuel cell outperformed its static performance, at point 2. At this point, the current and potential of the fuel cell are higher than the steady-state values. The underlying reasons for this dynamic behaviour cannot be assessed, as details of the controller are unknown. Similar observations were, however, made in Ref. [14], where it was suggested that hydration dynamics on the same timescales could be responsible. The authors of Ref. [14] hypothesized that the low stack temperature at the moment of the power ramp-up reduced the evaporation rate at the cathode. As more liquid water remained in the membrane, the fuel-cell over-potential was reduced at point 1. When the temperature increased and the water evaporated, the fuel-cell operating point moved to point 2. When the power was reduced to 200 W, the fuel-cell operating point moved closer to the steady-state operating line (point 3).

When the engine was throttled back to 100 W for the loitering phase, a similar phenomenon occurred. As the fans were still operating at the higher speed required for 200 W, the temperature dropped below the steady-state value initially, but recovered to a condition with a higher over-potential (point 4). As the fuel cell was then recharging the battery and delivering more power than in steady state, the voltage was slightly higher than the stationary value. Once the recharging reduced, the operating point moved close to the stationary polarisation curve. Similar phenomena occurred at points 5 and 6. The spread of the maroon-coloured points near point 6 occurred because the fuel cell recharged the battery again during descent. As a consequence, it took ~3–4 min for the temperature to drop to a steady value (not shown in Figure 11).

A similar behaviour was observed for the fast-cruise mission. Despite the higher power required (180 W, instead of 100 W), the fuel cell also settled at 20 min to its steady-state operating condition. The battery voltage, however, only increased to 23.4 V, instead of to 23.7 V. When a 2-min, 600-W climb was used, the overall voltage levels were very similar to the previously indicated values, as a shorter 200-W climb phase was required afterwards to reach the same cruising altitude. It however took ~16–18 minutes for the fuel cell to reach its steady-state operating condition.

5 Conclusion

This paper presents a HWIL-simulation architecture for testing of a fuel-cell-based hybrid power plant for small UAVs. For this study, the embedded hardware consisted of an Aeropak fuel-cell, its controller, a Li-Po battery pack and the Aeropak's power-management board. Several tests of the performance and endurance of the Aeropak system were performed using an electronic load to draw power from the system as well as to ascertain performance of a representative UAV mission.

It was shown that the fuel flow varied linearly with the fuel-cell power under steady-state conditions and that the fuel-cell efficiency was 55% at 40–200 W at steady state. The tests revealed that the dynamic performance of the system could differ significantly from this steady-state model and that the fuel cell could outperform its static operating point at high power settings. The tests also showed that the use of the battery in the hybrid system was key to the responsiveness of the system. The fuel cell was slower to transition to the higher power rating, and the battery compensated by initially delivering a slightly higher current.

The HWIL testing will be expanded next by adding high-frequency measurements of ancillary battery voltage and current to enable better characterisation at full-load conditions and during battery recharging. A brushless DC motor will also be added so that interactions between the fuel-cell-based hybrid-power-generation system and the motor can be evaluated.

References

[1] Shin Y, Chang S-H, *et al.* Performance test and simulation of a reciprocating engine for long endurance miniature unmanned aerial vehicles. *Proc Inst Mech Eng, Pt D: J Auto Eng*, Vol. 219, No. 4, pp. 573–581, 2005.

[2] Thomas JP, Qidwai MA, *et al.* Energy scavenging for small-scale unmanned systems. *J Pwr Src*, Vol. 159, No. 2, pp. 1494–1509, 2006.

[3] Palmer JL. Energy alternatives for unmanned aerial vehicles. *Land Warf Conf Proc*, Brisbane, QLD, Australia, VP Puri and D Filippidis, eds., pp. 161–183, 2008.

[4] Verstraete D, Steimes J, *et al.* Conceptual design of a PEM fuel cell powered unmanned aerial vehicle. *Proc 8th Ntl Cong Theo App Mech*, Brussels, Belgium, 2009.

[5] Kim M-J and Peng H. Power management and design optimization of fuel cell/battery hybrid vehicle. *J Pwr Src*, Vol. 165, No. 2, pp. 819–832, 2007.

[6] Burke AF. Batteries and ultracapacitors for electric, hybrid, and fuel cell vehicles. *Proc IEEE: Elec Hyb Fuel Cell Veh*, Vol. 95, No. 4, pp. 806–820, 2007.

[7] Bataller-Planes E, Lapeña-Rey N, *et al.* Power balance of a hybrid power source in a power plant for a small propulsion aircraft. *IEEE Trans Pwr Elec*, Vol. 24, No. 12, pp. 2856–2866, 2009.

[8] Horizon Energy Systems, Pte. Ltd. *The dawn of hydrogen fuel cell flight*. 2012. Available at: www.hes.sg.

[9] EnergyOR Technologies, Inc. *Fuel cell systems*. 2012. Available at: www.energyor.com.

[10] Bradley TH, Moffitt BA, *et al.* Flight test results for a fuel cell unmanned aerial vehicle. *Proc 45th AIAA Aero Sci Mtg*, Reno, NV, USA, Vol. 1, Paper AIAA-2007-32, pp. 254–261, 2007.

[11] Bradley TH, Moffitt BA, *et al.* Development and experimental characterization of a fuel cell powered aircraft. *J Pwr Src*, Vol. 171, No. 2, pp. 793–801, 2007.

[12] Horizon Energy Systems, Pte. Ltd. *Aeropak Technical Data Sheet*. 2010. Available at: http://www.hes.sg/files/AEROPAK_Technical_Data_Sheet.pdf.

[13] Palmer JL, Ashman DM, *et al.* Preliminary flight testing of autonomous soaring with the Kahu UAS. *Proc AIAC14*, Melbourne, VIC, Australia, 2011.

[14] Palmer JL. *Assembly and initial analysis of a database of the characteristics and performance of unmanned aerial systems*. Report DSTO-TR (in preparation), Air Vehicles Division, Defence Science and Technology Organisation, January 2012.

[15] Adams M and Halliop W. Aluminum energy semi-fuel cell systems for underwater applications: The state of the art and the way ahead. *Oc Conf Rec*, Biloxi, MS, USA, Vol. 1, pp. 199–202, 2002.

[16] Larminie J and Dicks A. *Fuel cell systems explained*. 2nd edition, John Wiley and Sons, Ltd., 2003.

[17] Santarelli M, Cabrera M, *et al.* Analysis of solid oxide fuel cell systems for more-electric aircraft. *J Acft*, Vol. 46, No. 1, pp. 269–283, 2009.

[18] LaBreche T. Solid oxide fuel cell power systems for small UAVs. *Jnt Srv Pwr Expo*, San Diego, CA, USA, 2007.

[19] NASA Dryden Flight Research Center. *Helios prototype: The forerunner of 21st century solar-powered "atmospheric satellites"*. 28 August 2002. Available at: http://www.nasa.gov/centers/dryden/news/FactSheets/FS-068-DFRC.html.

[20] Aerovironment details new Global Observer variants. *Flightglobal*, 14 February 2006. Available at: http://www.flightglobal.com/articles/2006/02/14/204655/aerovironment-details-new-global-observer-variants.html.

[21] Aerovironment, Inc. *Statospheric persistent UAS: Global Observer*. 2008. Available at: http://www.avinc.com/uas_product_details.asp?Prodid=35.

[22] Dovis F, Magli E, *et al.* HeliNet: Project status and the way forward. *Proc SPIE, Airb Recon XXV*, San Diego, CA, USA, WG Fishell and AA Andraitis, eds., Vol. 4492, pp. 21–28, 2001.

[23] Romeo G, Frulla G, *et al.* HELIPLAT: Design, aerodynamic, structural analysis of long-endurance solar-powered stratospheric platform. *J Acft*, Vol. 41, No. 6, pp. 1505–1520, 2004.

[24] Cestino E. Design of solar high altitude long endurance aircraft for multi payload and operations. *Aero Sci Tech*, Vol. 10, No. 6, pp. 541–550, 2006.

[25] Hendrick P, Hallet L, *et al.* Comparison of propulsion technologies for a HALE airship. *Proc 7th AIAA Avia Tech Int Ops Conf*, Belfast, Northern Ireland, Vol. 1, Paper AIAA-2007-7747, pp. 527–534, 2007.

[26] Frulla G and Cestino E. Design, manufacturing and testing of a HALE-UAV structural demonstrator. *Comp Struc*, Vol. 83, No. 2, pp. 143–153, 2008.

[27] Campbell DJ. Revolutionary propulsion and power for 21st century aviation. *Proc AIAA/ICAS Intl Air Spc Symp Expo*, Dayton, OH, USA, Paper AIAA-2003-2561, pp. 425–443, 2003.

[28] Sehra AK and Whitlow Jr W. Propulsion and power for 21st century aviation. *Prog Aero Sci*, Vol. 40, No. 4–5, pp. 199–235, 2004.

[29] Breit J and Szydlo-Moore J. Fuel cells for commercial transport airplanes needs and opportunities. *Technical Papers — 45th AIAA Aerospace Sciences Meeting*, Reno, NV, USA, Vol. 23, Paper AIAA-2007-1390, pp. 16413–16420, 2007.

[30] Boeing Phantom Works, Boeing Research & Technology — Europe. *Boeing prepares fuel cell demonstrator airplane for ground and flight testing*. 27 March 2007. Available at: http://www.boeing.com/phantom/news/2007/q1/070327e_nr.html.

[31] Lapeña-Rey N, Mosquera J, *et al.* The Boeing Fuel Cell Demonstrator airplane. *Proc SAE Aero Cong Ex*, Los Angeles, CA, USA, Paper 2007-01-3906, 2007.

[32] Romeo G, Moraglio I, *et al.* ENFICA-FC: Preliminary survey & design of 2-seat aircraft powered by fuel cells electric propulsion. *Proc 7th AIAA Avia Tech Int Ops Conf*, Belfast, Northern Ireland, Vol. 1, Paper AIAA-2007-7754, pp. 602–616, 2007.

[33] Politecnico di Torino. *ENvironmentally Friendly Inter City Aircraft powered by Fuel Cells (ENFICA–*

FC). 6 March 2008. Available at: http://www.enfica-fc.polito.it/en.

[34] Sanders V. On a wing and a fuel cell. *WPI Transf*, Fall 2002. Available at: http://www.wpi.edu/News/Transformations/2002Fall/onawing.html.

[35] Wentz WH, Myose RY, *et al.* Hydrogen-fueled general aviation airplanes. *Proc AIAA 5th Av Tech Int Ops*, Arlington, VA, USA, Vol. 1, Paper AIAA-2005-7324, pp. 230–242, 2005.

[36] Harvey JR and Palmer JL. *Characterisation of a PEM fuel-cell system with a focus on UAS applications*. Report DSTO-TR (in review), Air Vehicles Division, Defence Science and Technology Organisation, January 2012.

[37] UltraCell Corporation. *UltraCell leading a revolution in mobile power: Technology, fuel cells*. 2008. Available at: http://www.ultracellpower.com/sp.php?xx25.

[38] Protonex Technology Corporation. *Protonex: Revolutionizing portable power*. 2012. Available at: http://www.protonex.com.

[39] Jadoo Power Systems, Inc. *New power, new possibilities*. 2010. Available at: www.jadoopower.com.

[40] Ultra Electronics Holdings, PLC. *Welcome to Ultra Electronics AMI*. 2012. Available at: www.ultra-ami.com.

[41] Uconsystem Corp. *Unmanned aerial vehicle (RemoEye-006)*. 2011. Available at: http://uconco.en.ec21.com/Unmanned_Aerial_Vehicle_RemoEye_006--865587_866976.html.

[42] BlueBird Aero Systems, Ltd. *Boomerang: Long endurance, fuel-cell powered mini UAV*. 2009. Available at: http://www.bluebird-uav.com/Products_Boomerang.html; http://www.bluebird-uav.com/PDF/Boomerang_brochure_2009.pdf.

[43] Mortimer G. *AeroVironment Puma small UAS achieves record flight of over nine hours using fuel cell battery hybrid system*. 6 March 2008. Available at: http://www.suasnews.com/2008/03/3301/aerovironment-puma-small-uas-achieves-record-flight-of-over-nine-hours-using-fuel-cell-battery-hybrid-system/.

[44] The Mako, A Class 2 unmanned aerial vehicle, soars with a Jadoo Power fuel cell system. *FuelCellsWorks*, 13 October 2009. Available at: http://fuelcellsworks.com/news/2009/10/13/the-mako-a-class-2-unmanned-aerial-vehicle-soars-with-a-jadoo-power-fuel-cell-system/.

[45] Stroman RO, Kellogg JC, *et al.* Testing of a PEM fuel cell system for small UAV propulsion. *42nd Pwr Src Conf Proc*, pp. 487–490, 2000.

[46] Kellogg JC. *Fuel cell propulsion for small UAVs*. November 2005. Available at: http://www.nrl.navy.mil/techtransfer/exhibits/uavinfosht.html.

[47] Boland R. *Experimental power system expands flight capabilities*. March 2006. Available at: http://www.afcea.org/signal/.

[48] Ion Tiger achieves UAV flight endurance milestone. *Jane's Unman Aer Veh Targ* 2009. Available at: http://www.janes.com/products/janes/defence/air/unmanned-aerial-vehicles-targets.aspx?pu=1&rd=janes_com.

[49] Hannover Fair. *Hy-Fly der Wasserstoffflieger*. 2005. Available at: http://www.hydrogenambassadors.com/hm05/forum/fh-wiesbaden.php.

[50] Herwerth C, Ofoma UC, *et al.* Development of a fuel cell powered UAV for environmental research. *Proc 44th AIAA Aero Sci Meet*, Reno, NV, USA, Vol. 5, Paper AIAA-2006-237, pp. 2851–2864, 2006.

[51] Johnsen FA. *California students join small circle of revolutionary fuel-cell fliers*. 5 October 2006. Available at: http://www.nasa.gov/vision/earth/improvingflight/fuel_cells.html.

[52] University of Michigan students set new UAV record. *Fuel Cell Today*, 12 November 2008. Available at: http://www.fuelcelltoday.com/online/news/articles/2008-11/University-of-Michigan-students.

[53] LaBreche T and Ernst N. Advanced hybrid fuel cell power systems for UAVs. *Proc AUVSI Unman Sys NA*, Washington, DC, USA, Paper 2009-1890, 2009.

[54] Kim K, Kim T, *et al.* Fuel cell system with sodium borohydride as hydrogen source for unmanned aerial vehicles. *J Pwr Src*, Vol. 196, pp. 9069–9075, 2011.

[55] Georgia Tech Research Institute. *Flying on hydrogen: Georgia Tech researchers use fuel cells to power unmanned aerial vehicle*. 2006. Available at: http://www.gtri.gatech.edu/casestudy/flying-hydrogen.

[56] Moffitt BA, Bradley TH, *et al.* Design and performance validation of a fuel cell unmanned aerial vehicle. *Proc 44th AIAA Aero Sci Meet*, Reno, NV, USA, Vol. 13, Paper AIAA-2006-823, pp. 9877–9896, 2006.

[57] Rhoads GD, Wagner NA, *et al.* Design and flight test results for a 24 hour fuel cell unmanned aerial vehicle. *Proc 8th Ann Intl Ener Conv Eng Conf*, Nashville, TN, USA, Paper AIAA-2010-6690, 2010.

[58] AV Hornet. *Jane's Unman Aer Veh Targ* 2010. Available at: http://catalog.janes.com/catalog/public/index.cfm?fuseaction=home.ProductInfoBrief&product_id=98136.

[59] Micro air vehicle flies under fuel cell power. *Jane's Intl Def Rev*, 2003.

[60] Unmanned aerial vehicles and drones. *Av Wk & Sp Tech*, Vol. 168, No. 1, pp. 114–122, 2008.

[61] Kaz T. *Successful first flight of the "HyFish" – A fuel cell model aircraft is in the air*. 3 April 2007. Available at: http://translate.google.com/translate?hl=en&sl=de&u=http://www.dlr.de/desktopdefault.aspx/tabid-

1/86_read-8329/&sa=X&oi=translate&resnum=2&ct=result&prev=/search%3Fq%3DErfolgreicher%2BErstflug%2Bdes%2Bhyfish%26hl%3Den.

[62] Keidel B. *Design and simulation of solar powered aircraft for year-round operation at high altitude*. Doktor-Ingenieurs thesis, Technische Universität München, 20 January 2000.

[63] Ofoma UC and Wu CC. Design of a fuel cell powered UAV for environmental research. *Proc AIAA 3rd Unman Unlim Tech Conf*, Chicago, IL, USA, Vol. 1, Paper AIAA-2004-6384, pp. 193–203, 2004.

[64] Baldock N and Mokhtarzadeh-Dehghan MR. A study of solar-powered, high-altitude unmanned aerial vehicles. *Acft Eng Aero Tech*, Vol. 78, No. 3, pp. 187–193, 2006.

[65] Himansu A, Freeh JE, *et al.* Hybrid solid oxide fuel cell/gas turbine system design for high altitude long endurance aerospace missions. *Proc 4th Intl ASME Conf Fuel Cell Sci Eng Tech*, Irvine, CA, USA, Vol. 2006, Paper 2006-97095, pp. 573–583, 2006.

[66] Nickol CL, Guynn MD, *et al.* High altitude long endurance air vehicle analysis of alternatives and technology requirements development. *Proc 45th AIAA Aero Sci Mtg*, Reno, NV, USA, Vol. 18, Paper AIAA-2007-1050, pp. 12653–12669, 2007.

[67] Nam T, Soban DS, *et al.* A generalized aircraft sizing method and application to electric aircraft. *Proc 3rd Intl Ener Conv Eng Conf*, San Francisco, CA, USA, Vol. 1, Paper AIAA-2005-5574, pp. 598–615, 2005.

[68] Moffitt BA, Bradley TH, *et al.* Design space exploration of small-scale PEM fuel cell long endurance aircraft. *Proc 6th AIAA Av Tech Int Ops Conf*, Wichita, KS, USA, Vol. 1, Paper AIAA-2006-7701, pp. 14–29, 2006.

[69] Bradley TH and Parek DE. Comparison of design methods for fuel-cell-powered unmanned aerial vehicles. *J Acft*, Vol. 46, No. 6, pp. 1945–1956, 2009.

[70] Stroman RO and Kahn AD. Development and integration of controls for a PEMFC powered aircraft. *ECS Trans*, Vol. 11, No. 1 PART 2, pp. 1493–1504, 2007.

[71] Kim T and Kwon S-J. Design and development of a fuel cell-powered small unmanned aircraft. *Intl J Hyd Ener*, Vol. 37, No. 1, pp. 615–622, 2012.

[72] Bradley TH, Moffitt BA, *et al.* Validated modeling and synthesis of medium-scale polymer electrolyte membrane fuel cell aircraft. *Proc 4th Intl ASME Conf Fuel Cell Sci Eng Tech*, Irvine, CA, USA, Paper 2006-97233, pp. 381–390, 2006.

[73] Bradley TH, Moffitt BA, *et al.* Hardware-in-the-loop testing of a fuel cell aircraft powerplant. *J Pwr Src*, Vol. 25, No. 6, pp. 1336–1344, 2009.

[74] Masson PJ, Brown GV, *et al.* HTS machines as enabling technology for all-electric airborne vehicles. *Supercond Sci Tech*, Vol. 20, No. 8, pp. 748–756, 2007.

[75] Pratt JW, Brouwer J, *et al.* Experimental performance of an air-breathing PEM fuel cell at high altitude conditions. *Proc 43rd AIAA Aero Sci Meet*, Reno, NV, USA, Paper AIAA-2005-0953, 2005.

[76] Güther V and Otto A. Recent developments in hydrogen storage applications based on metal hydrides. *J All Comp*, Vol. 293, pp. 889–892, 1999.

[77] Oman H. Fuel-cell powered airplane propulsion. *IEEE Aero Elec Sys Mag*, Vol. 19, No. 1 I, pp. 12–13, 2004.

[78] Pogue WR, III, Baucom JN, *et al.* Structure-power system for unmanned air vehicles. *Proc AUVSI Unman Sys NA*, pp. 1155–1169, 2005.

[79] *Korean scientists build fuel cell-powered unmanned aircraft*. 2007. Available at: http://www.barnardmicrosystems.com/L4E_fuel_cell_flight.htm.

[80] Zhuo J, Chakrabarti C, *et al.* Dynamic power management with hybrid power sources. *Proc 44th ACM/IEEE Des Automat Conf*, San Diego, CA, USA, Paper DAC.2007.4261305, pp. 871–876, 2007.

[81] Fathy HK, Filipi ZS, *et al.* Review of hardware-in-the-loop simulation and its prospects in the automotive area. *Proc SPIE: Mod Sim Mil App*, K Schum and AF Sisti, eds., Vol. 6228, pp. 1–20, 2006.

[82] ITECH Electronics Co., Ltd. *User's Guide, Programmable DC electronic load IT8513B/IT8514B/IT8513C/IT8514C/IT8514F*. January 2010. Available at: http://www.itech.sh/null/IT-DOC/IT851314-UM-EN.pdf.

[83] Brian G, Young M, *et al.* The quest for a unified aircraft dataset format. *SimTect*, Sydney, NSW, Australia, 2005.

Acknowledgments

The authors thank Joshua Barnes for his contributions to the hardware-in-the-loop bench development as part of his thesis project at The University of Sydney. Geoff Brian at the Air Vehicles Division of the Australian Defence Science and Technology Organisation is greatly acknowledged for the provision of the flight simulator data on which the flight test results are based.

Copyright Statement